Composites: Part B 56 (2014) 34–41

Contents lists available at ScienceDirect

Composites: Part B

journal homepage: www.elsevier.com/locate/compositesb

Strain monitoring of composite elements by fibre Bragg grating sensors during a quasi-static indentation

V. Antonucci [a,b], M. Esposito [a], M.R. Ricciardi [a], M. Giordano [a,b], M. Zarrelli [a,*]

[a] Institute for Composite and Biomedical Materials, CNR, P.le Enrico Fermi, 1 80055 Portici, Italy
[b] Imast – Technological District on Polymeric and Composite Engineering Structures, P.le Enrico Fermi, 1 80055 Portici, Italy

ARTICLE INFO

Article history:
Received 2 May 2013
Received in revised form 18 June 2013
Accepted 15 July 2013
Available online 6 August 2013

Keywords:
A. Polymer–matrix composites (PMCs)
B. Debonding
E. Resin flow

ABSTRACT

The damage resistance of a fibre reinforced composite materials subjected to a concentrated indentation force has been investigated. Composite samples were manufactured by vacuum infusion process and then tested according to the concentrated quasi-static indentation test standard (QSI). The composite coupons were sensorized with embedded Bragg grating fibres in various positions, to monitor the indentation-induced deformations during the loading event. Numerical simulations, performed by using a commercial FEM software, were carried out and predictions results compared with experimental data.

Final results showed that Bragg wavelength changes sensitively depending on the applied quasi-static forces and it identifies correctly the non-linear pattern of the force–displacement curve. It was determined that strain transfer to the Bragg fibre is strongly influenced by the embedding conditions and final location of the optoelectronic sensors in term of shifting and in-plane rotation. Comparison between simulated and experimental data showed some discrepancy mainly due to the displacement of the embedded fibre sensors from their original location, caused by the manufacturing. However, by an inverse procedure based on iso-strain curves both shifting and rotation of the FBG sensors respect to their original position could be evaluated.

This work confirms that although Bragg fibres are effective and reliable to monitor deformations of composite elements during an impact event but unwanted and unpredictable effects, due to manufacturing, should be carefully taking into account to analyse correctly the sensor signal and quantitatively evaluate the inter-laminar strains.

1. Introduction

Polymer based composite materials have significant interest and they find several engineering applications in many industrial sectors, such as automotive, aeronautic, civil, naval. The optimal design of composite structures requires the use of numerical tools able to perform accurate stress analysis and predict the mechanical behaviour under specified load conditions. Therefore, laminated composite plates and shell elements are available in most of commercial finite-element codes in order to simulate the composite nature.

In general, several authors have focused the attention on the numerical study of the impact behaviour of composites panels by using finite element (FEM) codes and the development of proper models for the delamination failure or the other composite damage mechanisms, such as matrix cracks, fibre–matrix debond, fibre fractures. However, the proper modelling of laminated composites is a not trivial task and it can be still considered an open research problem due to the complex and anisotropic behaviour of composites. In order to assess the validity of FE models, it is important to perform experimental measurements that could provide useful information to validate the numerical results and help to develop predictive models for the mechanical behaviour of the composite material. Some of the main concerns, in aerospace and automotive material sciences, is the capability to design and realize composite laminates with low impact damage and high damage resistance and residual strength. Damage resistance is the ability of a composite material to resist certain potential damage induced events. ASTM D6264-98 [1], standard test method for measuring the damage resistance of a fibre-reinforced polymer–matrix composite to a concentrated quasi static indentation force, can be adopted to simulate low-velocity/large-mass impact obtaining quantitative measurements of the damage resistance. According to the standard, an indentation force is applied to the composite laminate by slowly pressing a hemispherical steel indenter into the surface. The test allows screening the materials for damage resistance or to inflict damage into a specimen for subsequent damage tolerance testing. In fact, from the QSI test, critical contact force and delamination onset energy (DOE) [2,3], which can be referred to the critical

* Corresponding author. Tel.: +39 081 7758845; fax: +39 081 7758850.
E-mail address: mauro.zarrelli@imcb.cnr.it (M. Zarrelli).

1359-8368/$ - see front matter © 2013 Elsevier Ltd. All rights reserved.
http://dx.doi.org/10.1016/j.compositesb.2013.07.020

energy to trigger the initial delamination, can be obtained. After the QSI test, generally, the damage level is detected by ultrasonic scan analysis to assess the extension of the induced delamination. Although this technique results efficient for laboratory analysis and for quality control, it cannot be applied during normal service life of the composite structures as inspected part needs to be taken out of service and often disassembled, therefore resulting uneconomical and difficult/impossible to implement. Optoelectronic sensor devices can be a interesting and promising alternative [4–7] to monitor the integrity of composite structure or elements providing in situ real-time strain measurements under both static and dynamic conditions. fibre Optic Bragg sensors (FBG) have been successfully used to monitor cure-induced strains in thermosetting resin [4], to identify the crack locations in carbon fibre-reinforced plastic (CFRP) [5], or to detect the delaminations in CFRP cross-ply laminates under static four-point bending [6].

Recently, FBG sensor have been successfully employed to measure coefficient of thermal expansion of polymer system at cryogenic temperature revealing interesting results [7]. Thus, FBG are becoming key elements for the development of intelligent structural health monitoring systems of large structures, such as trains [8], wing box [9,10], submarine [11] in order to prevent catastrophic disasters.

In this study, the displacement and strains of composite plate under a concentrated indentation force has been investigated by using embedded Bragg fibre sensor at different interply locations. The performed test was carried out according to the ASTM D6264 standard and sensor signal compared with numerical results. In particular, the numerical simulations have been performed by using commercial FEM code, namely Comsol Multiphysic. The Bragg sensors were embedded within the composite laminates during the manufacturing process in two symmetric locations in order to monitor induced strains under both tensile and compressive stress state. The FBG data were compared with the corresponding numerical deformations and a good agreement has been obtained by taking into account both a shifting and a rotation of the FBG sensors. An inverse procedure based on iso-strain curves was implemented by matching the measured deformation values to identify the final location of FBG sensors within the composite element. Final results reveal that the sensor both shift and rotate during he manufacturing strongly effecting the signal.

2. Materials and experimental methods

The composite elements were manufactured by Vacuum Infusion Process (VIP) in our lab. The employed technology consists of fibre reinforcement impregnated by a thermosetting liquid resin driven by vacuum (VIP, vacuum infusion process). After the complete impregnation the composite, consolidation at 85 °C for 45 min occurs due to resin polymerization reaction of the matrix.

In this study, the commercial unsaturated pre-promoted polyester resin Arotran Q6530 by Ashland Inc. was mixed with 1 wt.% of MEKP curing agent and later vacuum infiltrated Chomarat UD glass fibre reinforcement (600 g/m^2).

Two different sets of composite coupons with stacking sequence $[90°/90°/0°]_s$ and $[90°/90°/45°]_s$ were manufactured. Before the manufacturing cycle, two FBG sensors were embedded through the reinforcement between the first and the second ply and the five and six ply at the centre of quarter laminate as shown in Fig. 1. The lamina mechanical properties, required as input for the FEM analysis, have been preliminary measured by testing composite sample manufactured in our processing lab according to the ASTM D3518 and ASTM D3039 standard, respectively, for shear and Young modulus. The used testing machine was an universal testing machine Instron 4202 equipped with 100 kN load cell. Composite samples

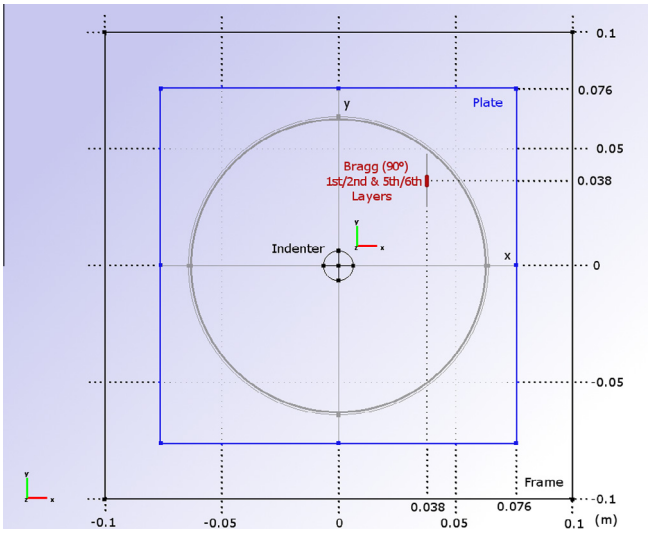

Fig. 1. Composite sample scheme along with FBG location.

were also instrumented by strain gauge rosettes for biaxial strain acquisition by using a Vishay D5000 rack system. Poisson coefficients v_{12} and v_{23} were measured by using strain gauges bonded on the composite samples.

3. The indentation test and the experimental FBG sensor measurement

The indentation tests have been carried out on composite panels characterised by two different lay-up, respectively $[90,90,0]_s$ and $[90,90,45]_s$, integrating two FBG sensors for each panel. A standard testing machine, Instron 8008, equipped with a hemispherical head penetrator device and a load cell of 10 kN was employed.

A centred load force was applied at 1 mm/min displacement rate on the sample located on a rigid support fixture located in the lower head of the testing machine (Fig. 2). The indenter has a smooth hemispherical tip with a diameter of 12.7 mm, while the fixture consists of a single plate with a 127.0 mm diameter opening. The specimen is 152 mm square and about 3 mm thick. Fig. 2 reports an image of the real experimental set up and a schematic solid model for the indented composite panel.

During the indentation test, the deformations along the fibre directions have been measured by two FBG sensors located between the first/s and fifth/sixth ply, respectively. Final signal of the FBG sensor can be directly correlated to the strain acting at sensor location during the indenter displacement. In its general form, the deformation curve results a function of the position (sensor location) and indenter vertical displacement:

$$\varepsilon = \varepsilon(\overline{X}, \delta) \tag{1}$$

where $\overline{X}$ and δ represent the coordinate position vector and the vertical displacement of the indenter, respectively (see Fig. 2).

The FBG sensors are tiny sensing elements (few hundreds of μm in diameter) which can be embedded into an element, without having almost any effect on the stress/strain field. Moreover, this type of sensor presents a further useful advantage, which make them ideal choice in a wide range of different industrial sectors and products with the potentiality of being used as an on-line and in-field monitoring tools. These sensors operate simply acting like selective mirrors that reflects a single wavelength of the light passing in the optic fibre. In fact, the Bragg operation relies on grat-

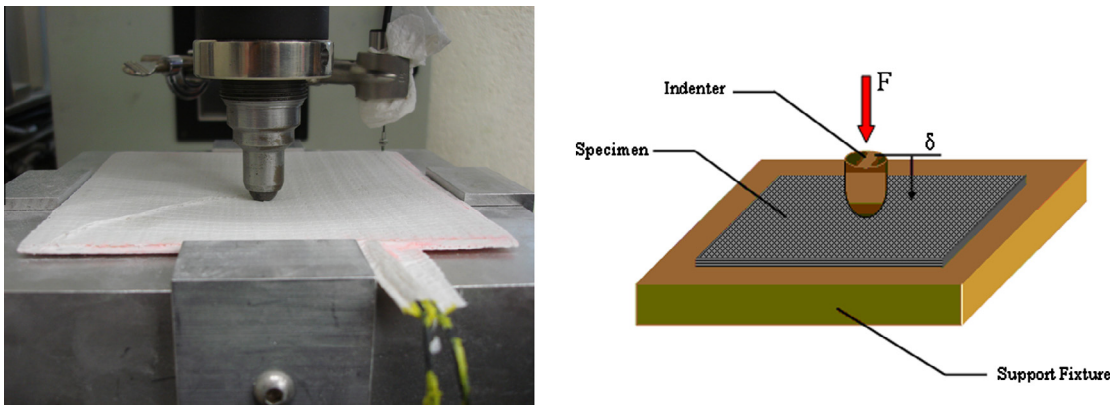

Fig. 2. Real and schematic quasi-static indentation test.

ing capability to reflect very narrow-band optical signal at a resonance wavelength λ_B given by:

$$\lambda_B = 2n\Lambda \tag{2}$$

where n is the refractive index of the core and Λ is the FBG grating pitch. It is well known that any factor (mechanical, thermal or other) capable of modifying the physical or geometric characteristics of the grating leads to a shift in the Bragg resonance wavelength and thus to a feed-back signal generation.

During each quasi static indentation test the sensor signals were acquired by using a MicronOptics sm25 system, with 4 optical channels at a resolution of 1 pm, an accuracy of 2 pm, a scan rate of 1 Hz. The connection between the signal acquisition device and the data storage was carried out by implementing a Labview interface. A schematic representation of the FBG set-up comprising both the interrogation and the acquisition system is reported in Fig. 3.

4. Experimental results

During the indentation test, the two FBG sensors are supposed to measure the deformations between the 1st–2nd and the 5th–6th ply, respectively, at in-plane position defined by the coordinate vector (original positions) reported in Table 1. For each configuration, three different panels were manufactured and tested, however, especially in the case of $[90,90,45]_s$ panels, early fracture or debonding of the sensor within the laminate have caused the rejection of these tests. For this reason, only $[90,90,0]_s$ panels were analysed and sensor signals compared with FEM predictions.

Figs. 4 and 5 report the measurements of the FBG sensors, in term of the wavelength, and corresponding load signal imported from the testing machine as function of the indenter displacement for a two $[90,90,0]_s$ panels (Fig. 4a and b) and $[90,90,45]_s$ panel

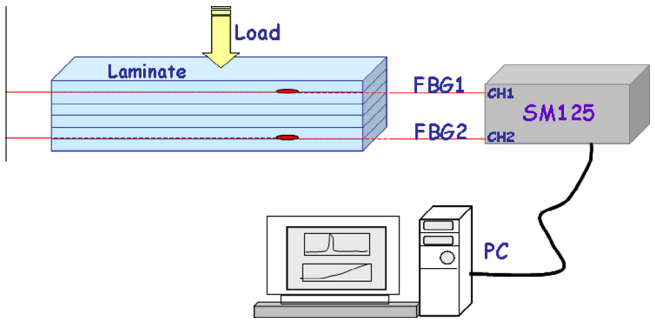

Fig. 3. Schematic representation of the experimental set-up.

Table 1
Location vectors for the FBG sensors in their original position and centre of laminate coordinates.

FBG1 positioned between 1st and 2nd ply	$\overline{X}_0^{1/2}(0.038, 0.038)$
FBG2 positioned between 5th and 6th ply	$\overline{X}_0^{5/6}(0.038, 0.038)$
Centre of the laminate	$\overline{X}_0(0.0, 0.0)$

(Fig. 5), respectively. As expected, in all cases the FBG between the 5th and 6th ply (*labelled Bragg 1 in blue colour*) shows compression strain while the sensor located at interface between 1st and 2nd ply (*labelled Bragg 2 in green*) records positive values according to the tensile strains acting into the composite at corresponding position. Before analysing any information from the recorded sensor signals, some considerations should be taken into account. Due to the different stages of the manufacturing process, the use of optoelectronic sensors, likely, face unwanted inconvenience related to debonding or "misallocation" from original designed position. Three cases could be suitably analysed comparing the different shapes of FBGs recorded patterns to the load cell signal during the indentation:

- sensors are correctly integrated within the laminate so the signal records the real strain acting at corresponding location (*case a*);
- sensors are completely integrated within the laminate but only up to a specific displacement values (*case b*);
- in the worst case, sensor signals does not follow the displacement progression due to unwanted debonding between fibre and laminate faced during the load puncture (*case c*).

In Fig. 4a, both FBG signals follow a non linear trend of induced strains which are congruent to the applied load. Deformation patterns are characterised by two different slopes with a change corresponding to the same value of the indenter displacement, which is around 3.7 mm. This result confirms that for the examined panel, the sensor is perfectly bonded to the laminate and its signal is tracking the induced strain throughout the loading pattern (*case a*). In the case of the sample 2 with lay-up $[90,90,0]_s$ (Fig. 4b), the slope change of the Bragg signal curves occurs for a lower value of the indenter displacement (as indicated on the figure) compared to the load inflection values. The different displacement value at which the slope for both load and FBG signal changes, is a directly related to the buoyancy of sensor bonding within the laminate (*case b*).

A complete debonding of the FBG sensor within the laminate is shown in the case $[90,90,45]_s$ panel (*case c in* Fig. 5). In fact, while

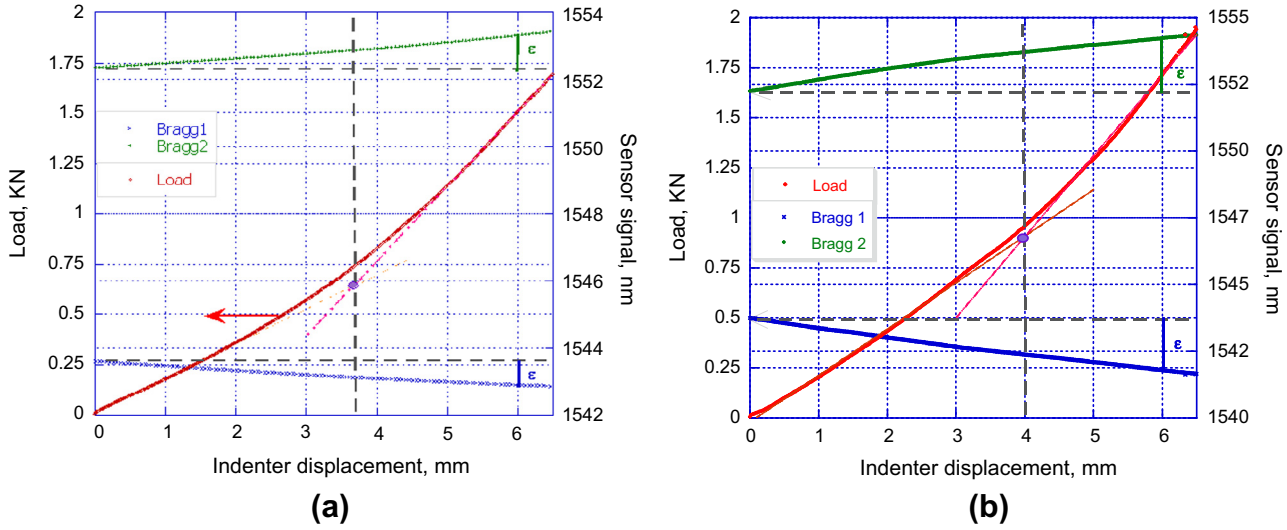

Fig. 4. FBGs and load signal for $[90,90,0]_s$ composite panels.

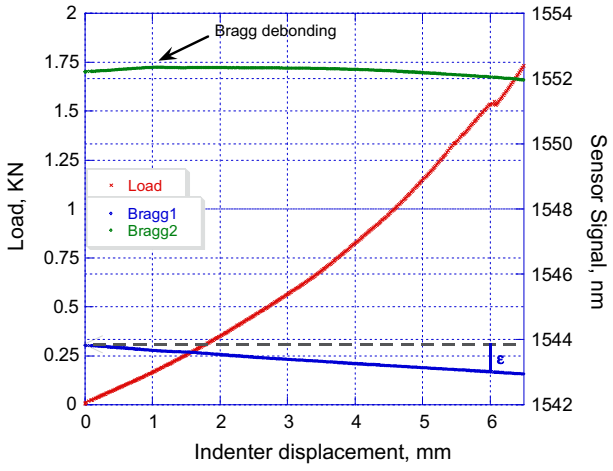

Fig. 5. FBGs and load signal for $[90,90,45]_s$ composite panel.

the FBG signal between the 5th and 6th ply correctly follows the compressive strain acting at that location within the laminate, during the loading stage, the FBG located between the 1st and 2nd ply shows a slightly increase up to 1 mm indenter displacement. For higher displacement values, adhesion interface between optoelectronic sensor and laminate is completely lost thus the signal records a plateau value although the indenter is still loading the sample. In the last stage of indentation, the signal reduces wrongly recording a compressive strain clearly inconsistent with the actual applied load. Data extract from FBG sensors have been used to evaluate the local deformation curves for both FBG sensor at corresponding positions ($\varepsilon_0^{1/2} = \varepsilon(\overline{X}_0^{1/2}, z_{\text{indenter}})$ and $\varepsilon_0^{5/6} = \varepsilon(\overline{X}_0^{5/6}, z_{\text{indenter}})$ respectively as function of the vertical indenter displacement) in the composite panels by monitoring the shift of the FBG sensors wavelength. Table 2 reports the deformation of the panel as measured by FBG sensor for an indenter displacement of 3 mm and for the original coordinate vector.

It is worth to note that the FBG signals value corresponding to 3 mm indenter's displacement is almost identical for panel 1 and 3, however in the case of panel 2, the value, recorded by the FBG sensor located between the 5th and 6th ply, increases abruptly. By noting, firstly, that the sign of the recorded value is congruent with the acting strain at that corresponding position, the relative

Table 2
Experimental deformations for a 3 mm indenter displacement.

$[90,90,0]_s$ PANEL LAY-UP		
Tested item	Deformation [με]	
	$\varepsilon_0^{1/2} = \varepsilon(\overline{X}_0^{1/2}, 0.003)\mu\varepsilon$	$\varepsilon_0^{5/6} = \varepsilon(\overline{X}_0^{5/6}, 0.003)\mu\varepsilon$
Tested item	Deformation [με]	
SAMPLE_1	396	−381
SAMPLE_2	n.a.	−426
SAMPLE_3	389	−376

difference between the signal value for 3 mm displacement can be reasonable attributed to a "misallocation" of the sensor itself. Handling of the dry preform or the laying-up procedure may likely cause a displacement of the sensor from its original position, thus the value of the inter-laminar strain is not corresponding.

5. Simulation predictions

The FEM simulations were performed by implementing the described test case in a commercial code, namely COMSOL Multiphysics v.3.4, considering a laminate of 6 plies characterised by the following lay-up: [90°–90°–0°–0°–90°–90°].

The resulting shear and Young modulus at 0° and 90° and Poisson coefficients ν_{12} and ν_{23} are reported in Table 3. The global FE model consists of three domains: composite panel, indenter and frame. The solid model for the simulated geometry along with jig frame is reported in Fig. 6.

Table 3
Lamina mechanical properties.

Property	Value
Young modulus E_1	37.09 (GPa)
Young modulus E_2	7.35 (GPa)
Poisson coefficient ν_{12}	0.185
Poisson coefficient ν_{23}	0.034
Shear modulus G_{12}	3.14 (GPa)
Tensile strength	660.29 (MPa)
Tensile strength	73.19 (MPa)
Maximum shear stress	44.07 (MPa)

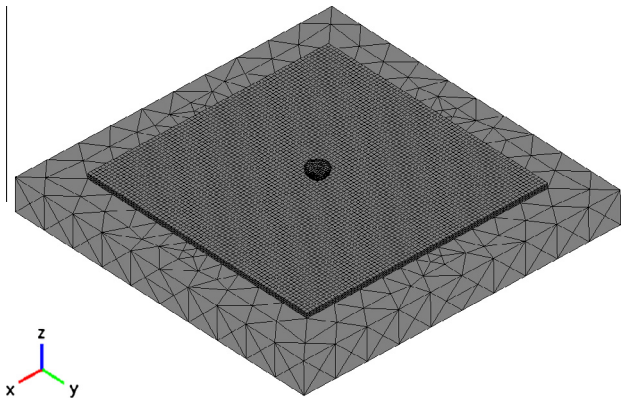

Fig. 6. Solid model for the FEM simulation.

Table 4
Numerical deformations at the centre of laminate quarter.

Lay-up	Element	Deformation [με]	
		$\varepsilon_0^{1/2} = \varepsilon(\overline{X}_0^{1/2}, 0.003)$	$\varepsilon_0^{5/6} = \varepsilon(\overline{X}_0^{5/6}, 0.003)$
$[90°-90°-0°]_s$	SOLID (Linear single-layer)	428	−525

The indenter and the frame have been assumed not deformable and a surface to surface contact (rigid to flexible) has been imposed between the indenter and the laminate and between the support plate and the laminate. Due to the symmetry of laminate [90°–90°–0°–0°–90°–90°] only a quarter of the element was considered. The deformations along the fibre direction between the first and second ply and between the 5th and 6th ply at the centre of the laminate quarter (see red point in Fig. 1) are shown in Table 4 for the analysed laminate configurations, for an indenter displacement of 3 mm and for the original sensor coordinate vector.

As expected, tensile deformations have been evaluated between the first and second ply and compression strains between the fifth and sixth ply.

6. Analysis and discussion

The numerical deformation values reported in Table 4 could be compared with corresponding experimental FBG measurements in Table 2. Strong differences are noticed for all composite panels. This can depend on manufacturing issues, such as the not correct orientation of the composite layers and the effective FBG position within the reinforcement. In fact, the resin flow can determine a displacement of the FBG sensor from its original position allowing both rotation and in-plane shifting. In the case of FBG rotation or/and shifting from their original position, the deformation data supplied by FBG sensors cannot be compared with simulated data extracted at the original positions. According to Eq. (2), in fact, being constant the vertical displacement of the indenter (i.e. 3 mm), the comparison between FBG data and FEM predictions should be made by matching the corresponding value at same in-plane location.

In order to establish the effective position of the FBG fibres within the reinforcement, before proceeding with the quasi-static indentation, each panel was carefully examined by monitoring the peak signal of the FBG sensor by a "tapping" procedure which allow a fast identification of the real FBG sensor location ($\overline{X}_{DBP}^{1/2}$ and $\overline{X}_{DBP}^{5/6}$ respectively for each sample, DBP stands for *Detected Bragg Procedure* as reported in Figs. 7 and 8) within the laminate after the manufacturing process and trimming phase. In particular, in the case of panel 1 with stacking sequence $[90,90,0]_s$, it was found that FBGs were located in the new positions $\overline{X}_R^{1/2} = (0.029, 0.041)$ and $\overline{X}_R^{5/6} = (0.033, 0.040)$, respectively, for the sensor located between the 1st/2nd and 5th/6th ply. An analogous procedure was performed to find the real position of the FBGs for the second and third panel having the same sequence (see Table 5).

The tapping procedure indeed may give a reasonable indication regarding the real position of the sensor in the final composite panel but of course it does not give any information on sensor rotation from its original direction which may occur during the manufacturing. Table 6 reports the coordinate of the FBG sensors for all the tested panel with $[90,90,0]_s$ stacking sequence, respectively initial and as-found after tapping procedure, $\overline{X}_0^{i/j}$ and $\overline{X}_{DBP}^{i/j}$. Therefore, the numerical deformations have been computed once more in these new locations by assuming that the FBG sensors were shifted from the centre of laminate quarter without any rotation. Table 5 reports the comparison for an indenter displacement of 3 mm at new position vectors.

Computing the strains at new locations, i.e. at tapping positions, $\overline{X}_{DBP}^{i/j}$, as defined in Table 5, at which the two sensors were supposed to move due to the manufacturing process, a significantly better agreement with experimental data was achieved. Nevertheless, still an significant discrepancy among the real and the computed strain values was attained. This could be likely attributed to the "conservative" assumption made on the displacement of the

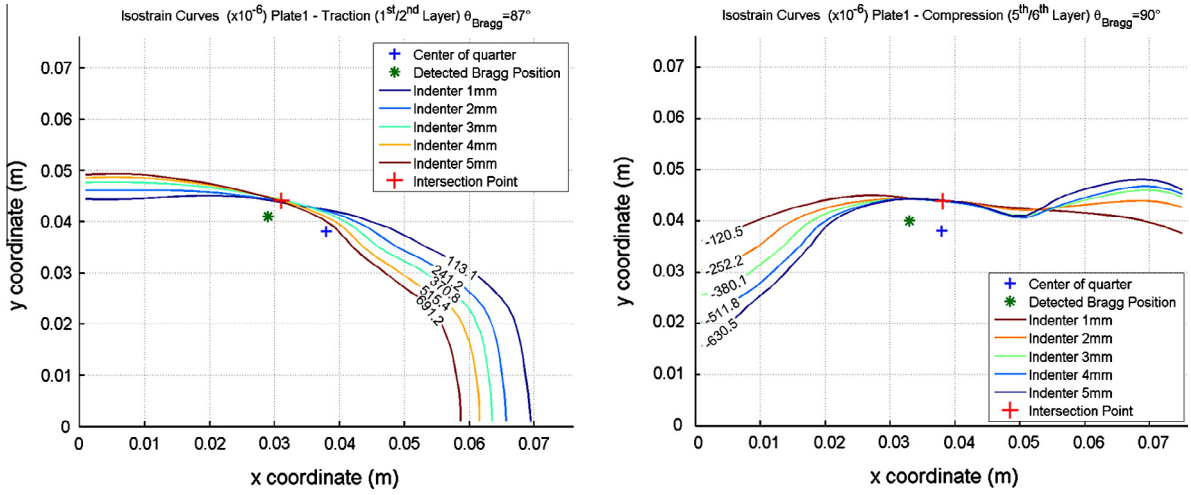

Fig. 7. Iso-strain curves at different indenter displacement steps for $[90/90/0]_s$ SAMPLE_1.

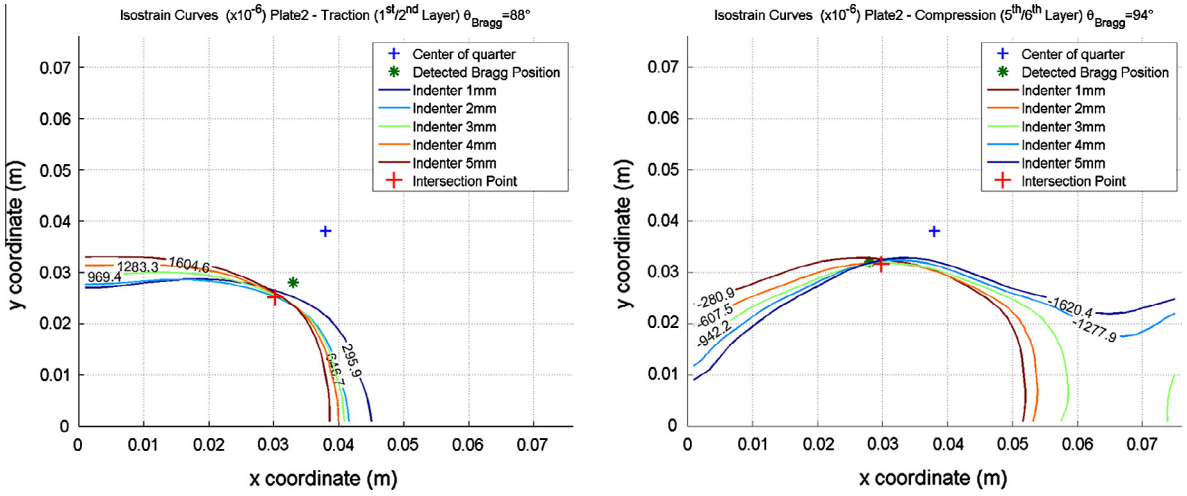

Fig. 8. Iso-strain curves at different indenter displacement steps for $[90/90/0]_s$ SAMPLE_2.

Table 5
Original vs. "tapping" position vector of FBGs for the $[90,90,0]_s$ tested panels.

$[90,90,0]_s$ PANEL LAY-UP		
SAMPLE_1	FBG location	Coordinate position vector
SAMPLE_2	1st and 2nd ply	$\overline{X}_0^{1/2} = (0.038, 0.038)$
SAMPLE_3	5th and 6th ply	$\overline{X}_0^{1/2} = (0.038, 0.038)$
${}_{SAMPLE\_1}\overline{X}_{DBP}^{1/2} = (0.029, 0.041)$	${}_{SAMPLE\_2}\overline{X}_{DBP}^{1/2} = (0.028, 0.032)$	${}_{SAMPLE\_3}\overline{X}_{DBP}^{1/2} = (0.029, 0.040)$
${}_{SAMPLE\_1}\overline{X}_{DBP}^{5/6} = (0.033, 0.040)$	${}_{SAMPLE\_2}\overline{X}_{DBP}^{5/6} = (0.033, 0.028)$	${}_{SAMPLE\_3}\overline{X}_{DBP}^{5/6} = (0.032, 0.041)$

sensors from their original location. In fact, the positioning of the FBG, after the manufacturing process, could be not only affected by a shift from its original position but also by an in-plane rotation, being the out-of-plane necessarily constrained by the presence of the plies. Supposing that the FBG sensor could both move and rotate within the laying plane, a computational procedure was implemented to evaluate real position of the sensor after the manufacturing process.

For this purpose, the numerically obtained iso-strain curves corresponding to five different indenter displacement within the range 1–5 mm, have been intersected each other in order to find a compatible FBG position. Indeed, the position of the FBG should be always the same for each registered value of the strain, however, considering only a shift of the FBG from its original position, the intersection point still results approximated. Therefore, in order to achieve a better precision of the real location of the FBG sensor, the evaluation of the iso-strain curves was performed by considering also different FBG rotation angles, obviously starting from their original orientation of 90°, i.e. along the orientation of the fibre reinforcement, and allowing a maximum variation of +/−5°.

Figs. 8 and 9 show the obtained optimal iso-strain curves and their intersection point (red colour) for the two panels, SAMPLE_1 and SAMPLE_3, respectively, being the value measured by the FBG sensor almost the same in the case of SAMPLE_1 and SAMPLE_2.

Each plot highlights the centre of laminate quarter (*blue coloured point*) and the "tapping" FBG location (*green coloured point*) and the intersection of iso-strain curve (*red coloured point*) which corresponds to the point where the strain evolution follows identically the same values as recorded by the FBG sensor. Therefore, this point represent the position of the FBG sensor within the panel at given inter-ply location during te whole indentation procedure.

Table 6
Comparison between numerical and experimental deformations for $[90,90,0]_s$ panel composites.

$[90,90,0]_s$ PANEL LAY-UP		Strain [με]	
Interlayer position	Tested item	Experimental	Numerical
1st/2nd ply	SAMPLE_1	396	$\varepsilon_0^{1/2} = \varepsilon(\overline{X}_T^{1/2}, 3mm) = 475$
	SAMPLE_2	395	
	SAMPLE_3	391	
5th/6th ply	SAMPLE_1	−384	$\varepsilon_0^{1/2} = \varepsilon(\overline{X}_T^{1/2}, 3mm) = 464$
	SAMPLE_2	−381	
	SAMPLE_3	−375	

Fig. 7(a) and Fig. 8(a) are relative to the iso-strain curves between the 1st and 2nd ply, while Fig. 7b and Fig. 8(b) report the iso-strain curves between the 5th and 6th ply.

The results reported in those plots, clearly revealed (a) that the sensor location according to the tapping procedure moved from their original location (b) that the tapping procedure obviously do not localise precisely the new FBG position nevertheless it identifies correctly the region where the sensor is positioned after the manufacturing process (c) that FBGs sensor result shifted and rotated from their original position according to the iso-strain intersection point as reported in Figs. 7 and 8.

The implemented inverse localization procedure could optimise the fibre location not only in term of in-plane displacement but also identified the most congruent rotation of the Bragg fibre from its longitudinal direction. In fact, due to the manufacturing, sensor can not only change their position from their original location but, being allocate between fibre tows, they can also rotate.

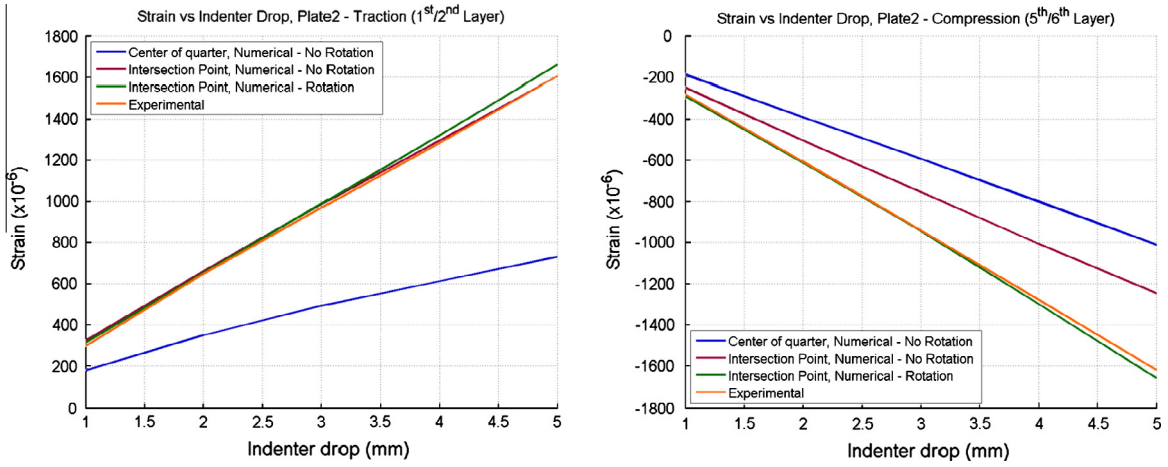

Fig. 9. Strain value vs. indenter vertical displacement for $[90/90/0]_s$ SAMPLE_2 panel.

Table 7
Position vectors of FBG sensor according to the iso-strain curve procedure.

${}_{SAMPLE\_1}\overline{X}_R^{1/2} = (0.031, 0.044)_{SAMPLE\_1}\theta_R^{1/2} = 3^\circ$	${}_{SAMPLE\_2}\overline{X}_R^{1/2} = (0.030, 0.025)_{SAMPLE\_2}\theta_R^{1/2} = 2^\circ$	${}_{SAMPLE\_3}\overline{X}_R^{1/2} = (0.031, 0.044)_{SAMPLE\_3}\theta_R^{1/2} = 1^\circ$
${}_{SAMPLE\_1}\overline{X}_R^{5/6} = (0.038, 0.043)_{SAMPLE\_1}\theta_R^{5/6} = 0^\circ$	${}_{SAMPLE\_2}\overline{X}_R^{5/6} = (0.029, 0.031)_{SAMPLE\_2}\theta_R^{5/6} = 4^\circ$	${}_{SAMPLE\_3}\overline{X}_R^{5/6} = (0.038, 0.043)_{SAMPLE\_3}\theta_R^{5/6} = 2^\circ$

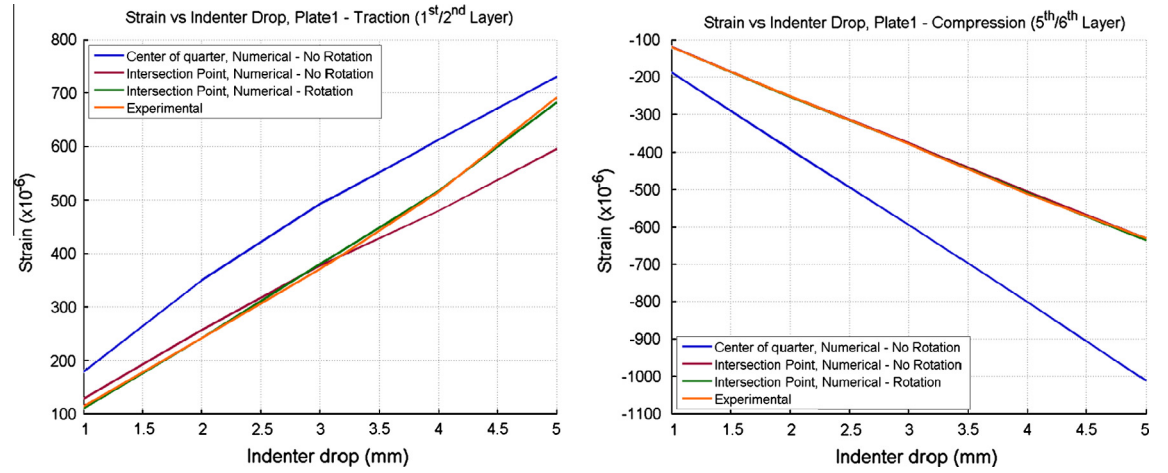

Fig. 10. Strain value vs. indenter vertical displacement for $[90/90/0]_s$ SAMPLE_1 panel.

Table 7 reports the coordinate vector, $\overline{X}_R^{i/j}$ and rotation angle, of the FBG found by the inverse iso-strain procedure for both sensors for each $[90/90/0]_s$ panel. In the case of the first panel, the FBG sensor placed between the first two plies results rotated by an angle of 3° while no rotation seems to occurre for the sensor located between the fifth and sixth ply. Almost the same data were obtained for SAMPLE_2. In this case, in fact, FBG sensor between the first two plies should be rotated from 90° to 88°, while the FBG sensor between the fifth and sixth ply is rotated by an angle of 4°. Finally, Figs. 9 and 10a/b show, as function of the indenter displacement, the comparison between the experimental deformations and the numerical strains, evaluated at the centre of laminate quarter and at the intersection point of the iso-strain curves with and without rotation of the sensors. The diagrams reported in Figs. 9 and 10 clearly outline the effect of the FBG rotation on the deformation patterns for the considered point. Experimental and numerical data show the same evolution if the rotation is taken into account, confirming the reliability of FBG sensors to monitor the deformations during quasi static impact however "unpredictable rotation" and "shift" can occur due to manufacturing affecting he buoyancy of sensor signal.

7. Conclusion

FBG sensor may represent a very suitable solution to monitor the strain curve during a quasi-static indentation. However careful consideration should be made when the analysis of the data is made. In fact, the tiny optoelectronic sensors which present many advantages compared with traditional sensor, could undergoing either shifting from their original position and/or rotation, mainly due to the manufacturing process (handling, layup, positioning and resin flow), which can strongly affect the final data analysis. Debonding of the sensors within the laminate could reduce or totally

invalidate their capability of strain monitoring. In our case, in fact, experimental results reveal some inconsistency with expected behaviour mainly due to poor adhesion with composite laminate; furthermore, it was observed that the changed position of the sensors with respect to their original position could strongly give arise to difference between experimental value and FEM predictions.

In conclusion, the performed numerical/experimental study demonstrated the capability of the FBG sensors to get in real time local information on the strain fields under specified load conditions. In the analysis of the results it results extremely important to point out that, in the case of composite materials, the sensor measurements can be affected by manufacturing issues, such as the position of the sensors, rotation and adhesion between sensor and composite laminate. For these reasons useful information on the effective composite mechanical behaviour should be always validate by a carefully analysis of the state of stress and loading conditions acting on the considered element.

References

[1] ASTM Designation. D 6264-98. Standard test method for measuring the damage resistance of a fibre-reinforced polymer–matrix composite to a concentrated quasi-static indentation force; 1998.
[2] Yi X-S, Hu Y, Tao X. Preliminary study on simultaneous measuring the force-depth-piezoresistance relation of carbon fibre polymer composites under quasi-static indentation conditions. J Mater Sci Lett 2001;20:1725–7.
[3] Gao Feng, Jiao Guiqiong, Zhixian Lu, Ning Rongchang. Mode II delamination and damage resistance of carbon/epoxy composite laminates interleaved with thermoplastic particles. J Compos Mater 2007;41:111–23.
[4] Antonucci V, Cusano A, Giordano M, Nasser J, Nicolais L. Cure-induced residual strain build-up in a thermoset resin. Composites: Part A 2006;37(4):592–601.
[5] Okabe Yoji, Tsuji Ryohei, Takeda Nobuo. Application of chirped fibre Bragg grating sensors for identification of crack locations in composites. Composites: Part A 2004;35:59–65.
[6] Takeda S, Okabe Y, Takeda N. Monitoring of delamination growth in CFRP laminates using chirped FBG sensors. J Intell Mater Sys Struct 2008;19:437.
[7] Esposito M, Buontempo S, Petriccione A, Zarrelli M, Breglio G, Saccomanno A, et al. fibre Bragg grating sensors to measure the coefficient of thermal expansion of polymers at cryogenic temperatures. Sens Actuat A 2013;189(195–20):3.
[8] Jang Byeong-Wook, Lee Jung-Ryul, Park Sang-Oh, Kim Chun-Gon, Kim Jung-Seok. A health management algorithm for composite train carbody based on FEM/FBG hybrid method. Compos Struct 2010;92:1019–26.
[9] Ryu CY, Lee JR, Kim CG, Hong CS. Buckling behavior monitoring of a composite wing box using multiplexed and multi-channeled built-in fibre Bragg grating strain sensors. NDT&E Int 2008;41:534–43.
[10] Di Scalea FL, Matt H, Bartoli I, Coccia S, Park GH, Farrar C. Health monitoring of UAV Wing skin-to-spar joints using guided waves and macro fibre composite transducers. J Intell Mater Syst Struct 2007;18(4):373–88.
[11] Kiddy JS, Baldwin CS, Salter TJ. Certification of a submarine design using fibre Bragg grating sensors. In: Proc SPIE, vol. 5388; 2004.